CDK2-based CDK7 mimic as a tool for structural analysis: Biochemical validation and crystal structure with SY5609

Jana Škerlová, Veronika Krejčiříková, Miroslav Peřina, Veronika Vojáčková, Milan Fábry, Vladimír Kryštof, Radek Jorda, Pavlína Řezáčová

PII: S0141-8130(24)09928-8

DOI: https://doi.org/10.1016/j.ijbiomac.2024.139117

Reference: BIOMAC 139117

To appear in: *International Journal of Biological Macromolecules*

Received date: 11 September 2024

Revised date: 19 December 2024

Accepted date: 21 December 2024

Please cite this article as: J. Škerlová, V. Krejčiříková, M. Peřina, et al., CDK2-based CDK7 mimic as a tool for structural analysis: Biochemical validation and crystal structure with SY5609, *International Journal of Biological Macromolecules* (2024), https://doi.org/10.1016/j.ijbiomac.2024.139117

CDK2-based CDK7 mimic as a tool for structural analysis: biochemical validation and crystal structure with SY5609

Jana Škerlová[1*], Veronika Krejčiříková[1], Miroslav Peřina[2], Veronika Vojáčková[2], Milan Fábry[1], Vladimír Kryštof[2,3], Radek Jorda[2*], Pavlína Řezáčová[1]

[1]Institute of Organic Chemistry and Biochemistry, Czech Academy of Sciences, Prague, Czech Republic

[2]Department of Experimental Biology, Faculty of Science, Palacký University Olomouc, Olomouc, Czech Republic

[3]Institute of Molecular and Translational Medicine, Faculty of Medicine and Dentistry, Palacký University Olomouc, Olomouc, Czech Republic

*correspondence: jana.skerlova@uochb.cas.cz, radek.jorda@upol.cz

Abstract

Cyclin-dependent kinases (CDKs) regulate cell cycle progression and transcription. CDK7 plays a pivotal role in cell division and proliferation, and the *CDK7* gene often exhibits mutations or copy number loss in cancer. Pharmacological targeting of CDK7 has been proposed as a cancer treatment strategy and several inhibitors are currently in clinical trials. As opposed to CDK2, the use of structure-assisted drug design for CDK7 has been limited. We present here CDK2m7, a CDK2-based CDK7 mimic created by mutagenesis of the CDK2 active site pocket. CDK2m7 can be produced in *E. coli* in a fully active complex with cyclin A2 in high yield and purity. CDK2m7 exhibits a shift in inhibitor selectivity from CDK2 to CDK7 and readily crystallizes. Therefore, it can be used in structure-assisted design of CDK7 inhibitors, as demonstrated by the crystal structure of the complex with inhibitor SY5609. CDK2m7 thus represents a simple and affordable platform for CDK7 rational drug design.

Keywords

cyclin-dependent kinase, inhibitor, SY5609, selectivity, X-ray crystallography, structure-assisted inhibitor design

Highlights

- CDK2m7 is a CDK7 mimic created by rational mutagenesis of the CDK2 active pocket

- CDK2m7 active site mutations result in inhibitor selectivity shift from CDK2 to CDK7
- CDK2m7 crystal structure with inhibitor SY5609 validates previous modelling studies
- CDK2m7 represents a simple and affordable model for CDK7 inhibitor development

Introduction

Cyclin-dependent kinases (CDKs) in cooperation with cyclins orchestrate various cellular processes, of which the promotion of the cell cycle progression and transcription have been shown to be fundamental [1, 2]. Interestingly, CDK7 and CDK12 perform dual functions and are required for both transcription and cell cycle control [3]. CDK7, binding its regulatory partners cyclin H and MAT1, is responsible for the phosphorylation and activation of specific cell cycle CDKs, thereby driving cell division and proliferation. As a component of the multi-subunit general transcription factor TFIIH, CDK7 plays a pivotal role in the phosphorylation of the C-terminus of RNA polymerase II at serine 5 and serine 7 and regulates transcription initiation [4, 5]. In addition, CDK7 controls co-transcriptional 5′-end capping of the nascent mRNA and through T-loop phosphorylation of CDK9, CDK12 and CDK13 can prime RNA polymerase II for subsequent phosphorylation to facilitate transcriptional elongation [2].

Transcriptional CDKs, including CDK7, exhibit significant copy number loss or mutations in cancer. Genomic analyses of thousands of tumor samples have revealed that *CDK7* losses correlate with increased sensitivities to DNA-damaging drugs [6]. Given that CDK7 preferentially regulates the expression of DNA damage response (DDR) genes and impairs the activity of homologous recombination (HR), pharmacological targeting *via* CDK7 inhibitors in HR-proficient tumors has been proposed as a strategy to treat cancer in combination with PARP inhibitors or other DNA-damaging agents [6].

Numerous highly potent and selective CDK7 inhibitors have been introduced, represented by classical ATP competitors (*e.g.* BS181, LDC4297 or samuraciclib), irreversible inhibitors attacking C312 of the CDK7 outside of the ATP cavity (*e.g.* THZ-1, mevociclib), or chimeric molecules responsible for E3 ligase-mediated degradation (*e.g.* PROTACs derived from YKL-5-124) [7-13] (Figure 1). To date, no CDK7 inhibitors have been approved as drugs, but several candidates entered clinical trials (*e.g.* TY-2699a, BTX-A51, LY3405105, Q901) , but their structures and relevant experimental data have not been disclosed yet [7, 14].

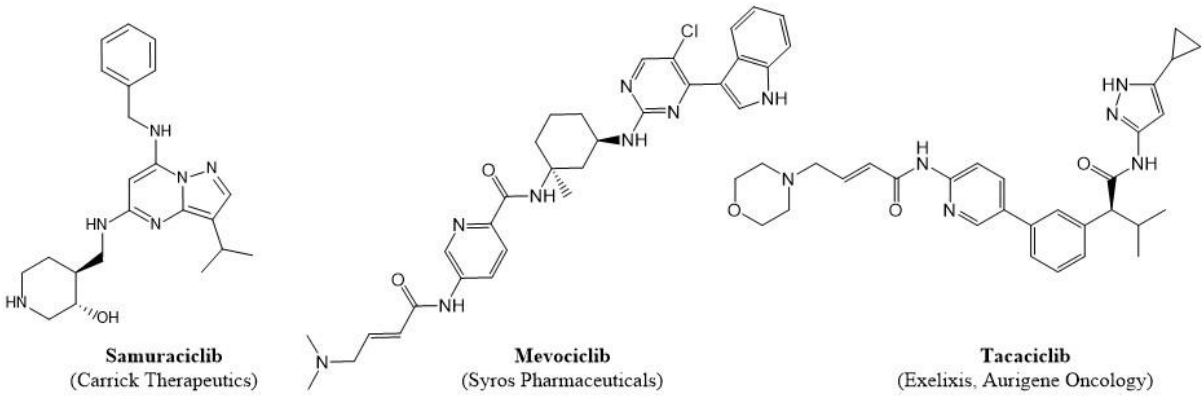

Figure 1. Examples of selective CDK7 inhibitors.

Structure-based drug design on CDK7 has not been extensively used due to the lack of a well-established structural biology platform for this kinase, especially when compared to CDK2. CDK2 can be easily expressed in a phosphorylated form in *E. coli* and co-purified with cyclin A2 [15]. There are over 400 structures of CDK2 in the Protein Data Bank (PDB) [16], and high-resolution structures with many inhibitors are available. CDK2 is therefore often used as a model for structure-assisted design of inhibitors of other CDKs. CDK7 requires expression in insect cells [17, 18], and until recently, there have been only few X-ray structures of CDK7 in the PDB – relatively low-resolution monomeric CDK7 in complex with ATP [17] and with inhibitor LDC4297 (PDB 8p4z, unpublished), and dual T-loop phosphorylated CDK7 in complex with cyclin H, MAT 1, and a camelid nanobody [19]. Only very recently, cryo-electron microscopy (cryo-EM) has been demonstrated to be suitable for structural studies of inhibitor binding to CDK7. High-resolution cryo-EM structures have recently been determined for CDK7 complexes with cyclin H and MAT 1 with adenosine 5'-O-(3-thio)triphosphate (ATP-gamma-S) and with a number of inhibitors including for example THZ1, samuraciclib (CT7001=ICEC0942), and dinaciclib [18, 20, 21]. Additional cryo-EM structures of CDK7 in large complexes including RNA polymerase are available, but they are unrelated to inhibitor design.

In this work, we present CDK2m7 – a CDK2-based CDK7 mimic that can be expressed in *E. coli* in a fully active phosphorylated form. Similar approach has been successfully used for several other kinases, including CDK4 [22], AKT [23], ROCK [24] and ATR [25]. We demonstrate that CDK2m7 can be purified in complex with a fragment of cyclin A2 with a yield and purity suitable for X-ray crystallography and we show the shift of selectivity from CDK2 to CDK7 in kinase assay, validating CDK2m7/cyclin A2 as a good mimic of CDK7 and a suitable model for co-crystallization with inhibitors. We also present the crystal structure of

CDK2m7 in complex with cyclin A2 and inhibitor SY5609, a selective CDK7 inhibitor currently undergoing clinical trials.

Material and Methods

Molecular cloning

The expression plasmid was constructed based on the design by D. Barford, J. Tucker, N.R. Brown and N. Hanlon (unpublished data). It is composed of two units, GST-tagged Civ1 and GST-tagged CDK2m7, both under the control of Ptac promotor. Civ1 is preceded by thrombin protease site, whereas CDK2m7 is preceded by PreScission protease site. Using the PreScission protease in the course of purification (see below) will thus release only CDK2m7, whereas GST-tagged Civ1 will be separated by binding to GST-Sepharose [15].

DNA coding for Civ1 kinase, obtained by PCR using yeast genomic DNA as template and primers that introduced BamHI, stop codon and EcoRI sites, was cloned as BamHI-EcoRI insert into modified pGEX6P1; the modification consisted in replacing the PreScission protease site by thrombin site.

To obtain CDK2m7, complete CDK2 coding region was first subcloned as BamHI-XhoI from pGEX6P1-CDK2 (Addgene, USA) into pBluescript. There, the synthetic DNA fragment BamHI – internal NheI (Eurofins Scientific, Luxembourg) and containing mutations specific for CDK2m7 was used to replace the corresponding region in CDK2. This modified DNA was put back into pGEX6P1 vector as BamHI-XhoI and served as a template for PCR with the primers having SalI at the 5′and NotI at the 3′, allowing amplification of the region spanning Ptac promotor, GST tag, and a complete coding region of CDK2m7. SalI-NotI fragment was then cloned into the Civ1-containing pGEX6P1 vector described above.

Protein expression and purification

The expression and purification procedure were based on a previously published protocol [15]. CDK2m7 was overexpressed from the pGEX6P1-based expression vector described above together with the Civ1 kinase, which phosphorylated CDK2m7 during the co-expression. The expression was performed in *E. coli* CONTROLLER BL21(DE3) at 37 °C in LB medium supplemented with 0.5% glycerol and 100 µg/mL ampicillin. At OD_{550nm} of 0.7, temperature was decreased to 18 °C and protein expression was induced with 100 µM ethyl-β-D-thiogalactopyranoside; the cultivation proceeded for 20 h.

A fragment of cyclin A2 (residues 175-432, gifted by Daniel Fisher, IGMM-CNRS, Montpellier, France) was overexpressed from a pET-21d(+)-based expression vector [26] in *E. coli BL21*(DE3) at 37 °C in LB medium supplemented with 0.5% glycerol and 100 µg/mL ampicillin. At OD_{550nm} of 0.5, temperature was decreased to 27 °C and protein expression was induced with 100 µM ethyl-β-D-thiogalactopyranoside; the cultivation proceeded for 4 h.

Cell paste from 3 liters of each the CDK2m7 and cycA cell cultures was processed separately as follows. The cycA-expressing cells were resuspended in 450 mL of 50 mM Tris pH 8.0, 300 mM NaCl completed with protease inhibitor cocktail (Clontech, USA). The CDK2m7-expressing cells were resuspended in 450 mL of purification buffer (40 mM HEPES pH 7.5, 200 mM NaCl, 0.02% monothioglycerol, 5 mM DTT) completed with protease inhibitors (Clontech, USA). The cells were lysed by Avestin Emulsiflex C3 (ATA Scientific Instruments, Australia), clarified by centrifugation (23,500 *g*, 4 °C, 1 h), and pooled together before purification by affinity chromatography. The combined lyzate was loaded on a home-made 15 mL GSTrap column (Cytiva, UK) pre-equilibrated in purification buffer using gravity flow. After washing the column with purification buffer, the bound complex was eluted with 20 mM glutathione in purification buffer. PreScission protease (Merck, Germany) was added in a 1:20 (w/w) ratio to the eluted protein and the cleavage was performed overnight at 4 °C. The cleaved protein was then concentrated to 11 mg/mL and fractionated by size-exclusion chromatography on a HiLoad 16/600 Superdex200 pg column (GE Healthcare, USA) and Äkta FPLC (GE Healthcare, USA) in the purification buffer. Fractions containing the CDK2m7/cycA complex were pooled, reloaded onto a GSTrap column to remove the GST, and the flowthrough containing pure CDK2m7/cycA was concentrated to 7.3 mg/mL and stored at -80 °C until further use. The purification procedure yielded 3.5 mg of pure CDK2m7/cycA complex per liter of CDK2m7 cell culture.

Crystallization

CDK2m7/cycA at the concentration of 7.3 mg/mL in 40 mM HEPES pH 7.5, 200 mM NaCl, 0.02% monothioglycerol, 5 mM DTT was mixed with 10 mM inhibitor SY5609 in 100% DMSO. The final protein and inhibitor concentration was 6.9 mg/mL and 0.65 mM, respectively, and the final protein:inhibitor molar ratio was 1:3. The sample was incubated for 45 min on ice and clarified by centrifugation (22,000 *g*, 4 °C, 15 min). The crystal of CDK2m7/cycA in complex with SY5609 was obtained by the sitting-drop vapor diffusion technique in Swissci 96-well 3-drop plates (Molecular Dimensions, USA) using the Oryx8

robot (Douglas Instruments, UK). The reservoir solution contained 30 µl of 0.8 M succinic acid pH 7.0 from the JCSG$^+$ Suite (Molecular Dimensions, USA). Crystallization drops were prepared by mixing 100 nl of the protein-inhibitor complex and 100 nl of the reservoir solution and incubated at 18 °C. Crystals appeared after 6 days and were harvested after 3 weeks and cryoprotected with 30% glycerol in the reservoir solution prior to flash-cooling in liquid nitrogen.

X-ray structure determination

Diffraction data were collected on beamline PX2a of Synchrotron SOLEIL and processed automatically in XDS [27]. The structure was solved by molecular replacement in Molrep [28] using the CDK2-cycA structure with the PDB code 7qhl [29] as the search model. The model was refined in Refmac [30] from the CCP4 package [31] in combination with manual adjustments in Coot [32]. Ligand geometry definition file was created by the program eLBOW [33] from the Phenix suite [34]. Electron density maps and model coordinates were deposited into the PDB [16] under the accession code 9GLA. Data collection and refinement statistics are listed in Table 1. Structural analysis of inhibitor binding was performed using the program CONTACT from the CCP4 package [31].

Kinase inhibition assay

Kinase assays with CDK2/cyclin A2, CDK9/cyclin T1 and CDK7/cyclin H/MAT1 complexes were assayed as previously described [35]. Briefly, CDK2m7/cyclin A2 kinase reactions were assayed with histone H1 as a substrate (1 mg/mL, Merck) in the presence of 1.5 µM ATP, [γ-^{33}P]ATP, and the test compound in a final volume of 10 µl of reaction buffer (100 mM HEPES-NaOH, pH 7.4, 3 mM $MgCl_2$, 3 mM $MnCl_2$, 3 µM Na-orthovanadate, 1.2 mM DTT, 2.5 µg/50 µl of $PEG_{20.000}$). Assays were performed at least in triplicate for 30 min using an Eppendorf ThermoMixer (350 rpm, 30 °C) in a 96-well format. The reactions were stopped by adding 5 µl of 3% aq. H_3PO_4. Aliquots were spotted onto P-81 phosphocellulose (Whatman), washed 3× with 0.5% aq. H_3PO_4 and finally air-dried. Kinase inhibition was quantified using a FLA-7000 digital image analyzer and IC_{50} values were determined from dose-response curves as the concentration of the test compounds required to reduce the activity by 50%. The concentration of ATP used in the kinase assay was determined based on the K_m value for ATP of each enzyme, which was determined for each kinase using a standard assay over an appropriate range of ATP concentrations. All assays were linear with respect to time and enzyme concentration under the conditions used.

Reagents

The collection of CDK inhibitors was purchased from MedChemExpress (ribociclib, SY5609, BS-181, LDC4297, JSH-150, CDK2-IN-4), Santa Cruz Biotechnology (RO-3306, NU6102), or Selleck Chemicals (samuraciclib).

Results and Discussion

Design of CDK2m7, a CDK2-based CDK7 mimic

The active pocket of cyclin-dependent kinases in general exhibits high plasticity, especially in the glycine-rich loop, and can accommodate a range of ligands with different chemical structures. To design mutations in the active site of CDK2 that would mimic CDK7, we have aligned selected ligand-bound structures of CDK2 and all structures of CDK7 available in the Protein Data Bank (PDB, RCSB.org) as of April 2023 [16] and identified CDK regions involved in contacts with ligands. We have then mutated the contact regions to the sequence of CDK7, except for those residues that had side-chains oriented away from the active pocket. The resulting CDK2 variant carries 12 mutations modifying the active pocket to mimic CDK7 (Figure 2) and is hereafter referred to as CDK2m7. CDK2m7 represents the first-choice design, i.e. the most extensive mutant, and we have not tested any other variants.

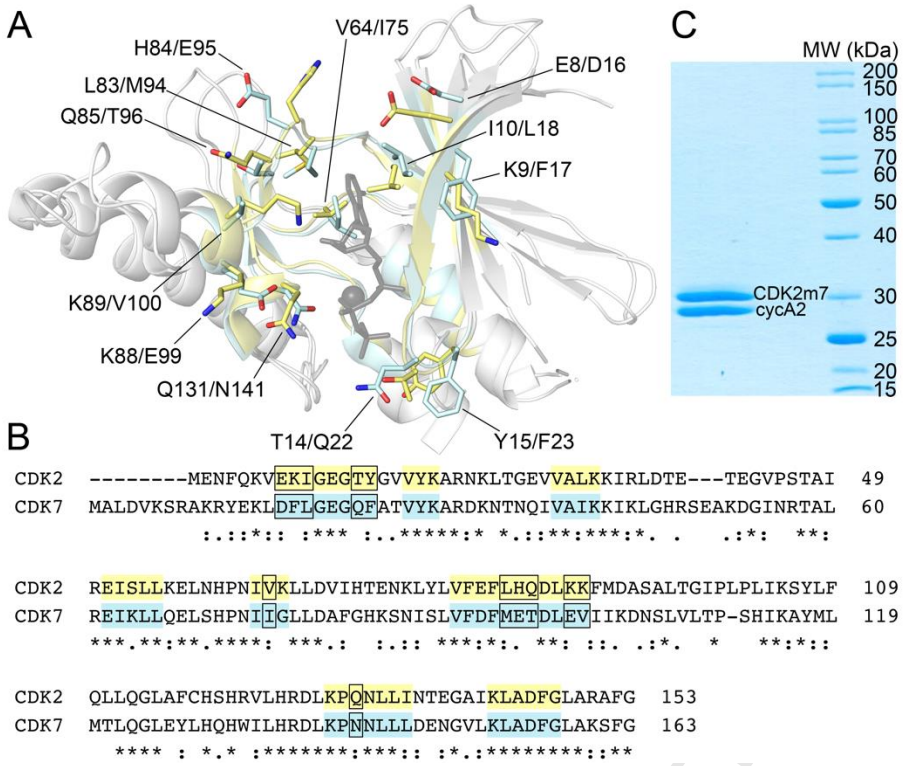

Figure 2. Design of CDK2m7. Structural (A) and sequence (B) alignment of N-terminal portions of CDK2 (PDB 8fp5 [36]) and CDK7 (PDB 1ua2 [17]). Regions forming the ligand-binding pocket are highlighted in yellow and cyan in CDK2 and CDK7, respectively. Mutated residues are shown as sticks with residues labelled in the CDK2/CDK7 order (A) and highlighted by boxes (B). The active site is marked by the ATP-Mg^{2+} complex from PDB 1ua2. Sequence alignment was created in Clustal Omega [37]. C. Coomassie-stained SDS-PAGE gel documenting the purity of the CDK2m7/cyclin A2 (cycA2) complex.

CDK2m7 can be expressed in *E. coli* in the Thr160-phosphorylated form and co-purified with a fragment of cyclin A2 (cycA, residues 175-432), separately expressed in *E. coli.* The simple purification protocol, which is described in detail in the methods section, combines affinity chromatography with size-exclusion chromatography and yields about 3.5 mg of pure and fully active CDK2m7/cycA complex per 1 liter of CDK2m7 cell culture (Figure 2C). In our hands, the complex readily crystallizes at concentrations around 7 mg/mL in conditions from the Morpheus and $JCSG^{+}$ crystallization screens. In addition, there are numerous structures of CDK2/cycA complexes in the PDB, with crystallization protocols applicable to CDK2m7/cycA. The expression, purification, and crystallization protocols presented here thus provide a simple and robust platform that can mimic CDK7 in structure-assisted design of CDK7 inhibitors.

Evaluation of inhibitor binding in CDK2m7

To confirm the suitability of the introduced mutations in CDK2m7, inhibitor binding was verified using a panel of CDK inhibitors with varying selectivity. Ribociclib (CDK4/6i), RO-3306 (CDK1i) and JSH-150 (CDK9i) were selected as compounds that should not target either CDK2 or CDK2m7 [38, 39]. Our results confirmed that the site-directed mutagenesis of the CDK2 active site pocket did not alter the preference of these tested inhibitors for the other studied CDKs (Figure 3). NU6102 and CDK2-IN-4, both nanomolar CDK2i [26, 40], displayed no inhibition of CDK2m7 (IC_{50} > 1 µM), which was also consistent with control data on the recombinant CDK7/cyclin H/MAT1 complex, confirming the effective modifications of the active site of CDK2. Finally, to demonstrate that CDK2m7 is a suitable model for structure-assisted design of CDK7 inhibitors, we tested several potent CDK7 inhibitors. SY5609 and BS-181 are described as selective CDK7 inhibitors [8, 41], which was confirmed also by our measurements (see Figure 3), where both showed no inhibition of CDK2 (IC_{50}'s > 1 µM), whereas CDK7 was effectively inhibited at nanomolar ranges (IC_{50}'s = 9 and 87 nM). We found that CDK2m7 was strongly inhibited by both inhibitors in nanomolar concentrations, although the IC_{50} values were ~ 6-fold higher than for CDK7. We also tested samuraciclib and LDC4297 [9, 10], which are published as CDK7 selective inhibitors, but with a lower selectivity index than SY5609 and BS181. Despite their low selectivity towards CDK7 in our hands (see Figure 3), both have retained single digit nanomolar values on CDK2m7.

Taken together, the abovementioned results demonstrate that the active site of CDK2m7 mimics well that of CDK7, and thus provides an estimation of the binding of CDK7 selective inhibitors.

Published preference	Inhibitor	IC_{50} for CDK/cyclin complexes (µM)			
		CDK2/A2	CDK9/T1	CDK7/H/MAT1	CDK2m7/A2 mimic
CDK1	RO-3306	0.233	>1 +	>1 +	>1 +
CDK2	NU6102	0.014	4.1	2.5	1.5
CDK2	CDK2-IN-4	0.032	9.4	>10 +	>10 +
CDK4/6	Ribociclib	>20 +	3.9	>10 +	2.9
CDK7	SY5609	4.04	0.744	0.009	0.041
CDK7	BS-181	1.3	1.8	0.087	0.566
CDK7	LDC4297	0.054	2.9	0.020	0.006
CDK7	Samuraciclib	0.059	0.138	0.014	0.014
CDK9	JSH-150	1.2	0.004	1.7	1.4

Figure 3. Kinase inhibition data expressed as IC_{50} values complemented by graphic illustration of the selectivity for certain CDK. Graphics (yellow and blue bars, + signs represent IC_{50} values above the highest tested level) illustrate CDK activity on a log10 scale where midpoint corresponds to 1 µM. The IC_{50} values were measured at least in triplicates.

Crystal structure of CDK2m7/cycA in complex with SY5609

We determined the crystal structure of active, Thr160-phosphorylated CDK2m7 in complex with a fragment of cyclin A2 and inhibitor SY5609 [41] (CDK2m7/cycA/SY5609) at the resolution of 2.2 Å. For data collection and refinement statistics, see Table 1. The asymmetric unit comprised one CDK2m7/cycA heterodimer with SY5609 bound in the active site (Figure 4). The quality of the electron density map allowed modeling of the complete protein sequence except for CDK2m7 residues 1, 39, and 295-298.

Table 1. Data collection and refinement statistics.

Values in parentheses refer to the highest resolution shell.

Data collection statistics	
PDB code	9GLA
Space group	$C222_1$
Cell parameters (Å; °)	a = 71.9, b = 109.8, c = 163.6; α = β = γ = 90
Number of molecules in AU	1
Wavelength (Å)	0.918
Resolution (Å)	48.47-2.18 (2.31-2.18)
Number of unique reflections	33,815 (5,245)
Multiplicity	13.3 (12.9)
Completeness (%)	99.3 (97.1)
R_{meas}	33.5 (393.1)
$CC_{(1/2)}$	99.6 (35.8)
Average I/σ(I)	9.5 (0.7)
Wilson B ($Å^2$)	52.4
Refinement statistics	
Resolution range (Å)	48.46-2.18 (2.24-2.18)
No. of reflections in working set	32,030 (2,112)
No. of reflections in test set	1,685 (110)
R value (%)	20.1 (57.9)
R_{free} value (%)	24.9 (57.2)
RMSD bond length (Å)	0.007
RMSD angle (º)	1.442
Number of atoms in AU	4,667
Number of protein atoms in AU	4,521
Mean B value ($Å^2$)	53.1
Ramachandran plot statistics	
Residues in favored regions (%)	96.9
Residues in allowed regions (%)	99.7

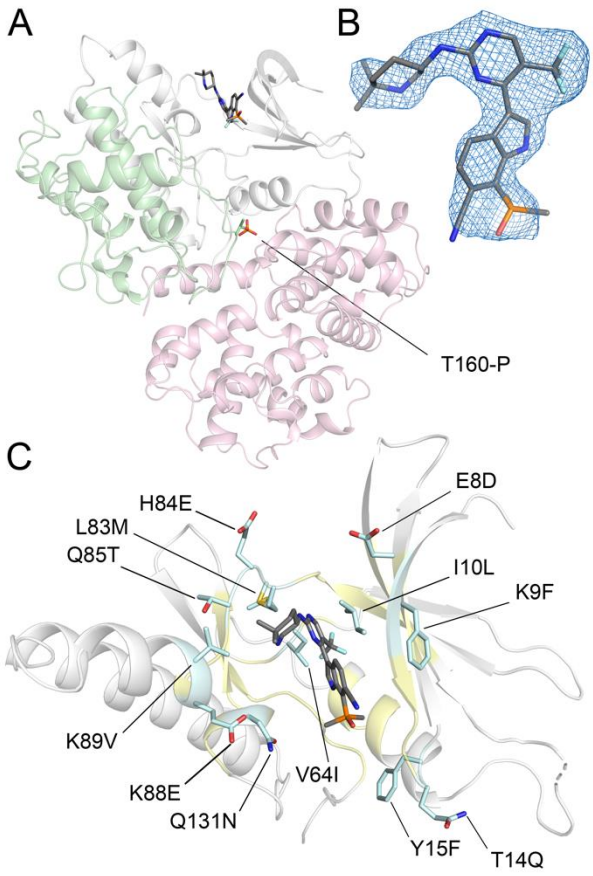

Figure 4. Crystal structure of CDK2m7/cycA/SY5609. A. Overall structure of the CDK2m7 (green and grey) complex with cycA (pink) and SY5609 (grey sticks). The position of phosphorylated Thr160 is indicated. The N-terminal portion of CDK2m7 surrounding the ligand-binding cleft (shown in detail in panel C) is colored grey. B. Simulated annealing omit map (2mF_o-DF_c) contoured at 1 σ is shown for SY5609. C. N-terminal portion of CDK2m7 is shown in a view corresponding to Figure 2A. Regions predicted to interact with ligands during the design of CDK2m7 are highlighted in yellow and mutated residues are shown as cyan sticks.

The inhibitor SY5609 binds to the active site cleft between the N-terminal and C-terminal domains of CDK2m7 and forms numerous hydrophobic and polar interactions with residues of the active site pocket subsites [42] (Figure 5). The amidopyrimidine moiety is sandwiched between Ala31 and Leu134 with further hydrophobic contribution of residues Leu10 and Phe82, and forms two conserved hydrogen bonds with the main chain atoms of the hinge-region residue Met83. The trifluoromethyl modification of the pyrimidine ring points to a protein interaction region outlined by Ile64, Ala144, and the main chain of Glu81, and stacks against the gatekeeper residue Phe80. The 6,6-dimethylpiperidine moiety is oriented along the main chain of Glu84 towards the "specificity-surface" residues Thr85, Asp86, and Val89. The

protonated, positively charged piperidine nitrogen forms a hydrogen bond and a salt bridge with Asp86. The indole moiety binds near Leu10 and is oriented towards the phosphate-ribose-binding pocket, stacking with Val18. The indole nitrogen interacts through a hydrogen bond with Asp145. The C6-nitrile modification on the indole points towards Gly11 and forms a water-mediated hydrogen bond with the main chain carbonyl of Glu12 from the glycine-rich loop. The dimethyl phosphine oxide moiety is relatively solvent-exposed and forms a weak C-H…O hydrogen bond with Asp145.

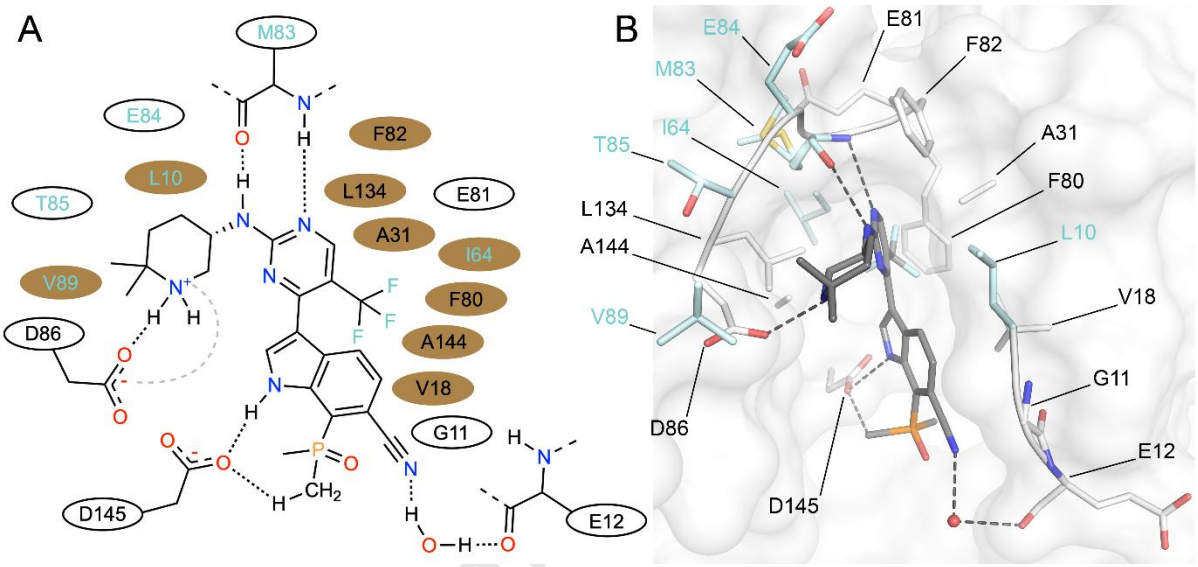

Figure 5. Interactions between CDK2m7 and SY5609. A. A schematic representation of the interactions between CDK2m7 and SY5609. Residues within van der Waals distance are shown, and mutated residues are labelled cyan and residues conserved between CDK2 and CDK7 are labelled black. Brown ovals indicate hydrophobic interactions. Hydrogen bonds are shown as black dotted lines and a salt bridge as a grey dashed line. B. A structural representation of the interactions between CDK2m7 and SY5609. Residues within van der Waals distance are shown as sticks below a semitransparent protein surface. Mutated residues are highlighted in cyan while residues conserved between CDK2 and CDK7 are colored white. Hydrogen bonds are shown as black dashed lines.

CDK2m7 maintains the integrity of the active site

To evaluate the suitability of CDK2m7 to serve as a structural tool for studies of CDK7 inhibition, we compared CDK2m7/cycA/SY5609 with available structures of inhibitor complexes of CDK7 (Figure 6) [18, 20] and with the structure of CDK2 with compound 4 from the inhibitor series leading to SY5609 (Figure 7) [41]. In case of CDK7, we selected structures

of the active CDK7 form in a complex with cyclin H and MAT 1 (CDK7/cycH/MAT1), and with non-covalent ligands; specifically, with adenosine 5'-O-(3-thio)triphosphate (ATP-gamma-S) [18], and with Samuraciclib (CT7001, ICEC0942) [20]. It is clear that the mutations do not disrupt the integrity of the active site and the side-chains of the mutated residues adopt conformations similar to those in the ligand-bound structures of the CDK7/cycH/MAT1 (Figure 6). Local differences in the ligand-binding residues can be attributed to accommodation of different ligands. This is especially noticeable in the flexible glycine-rich loop.

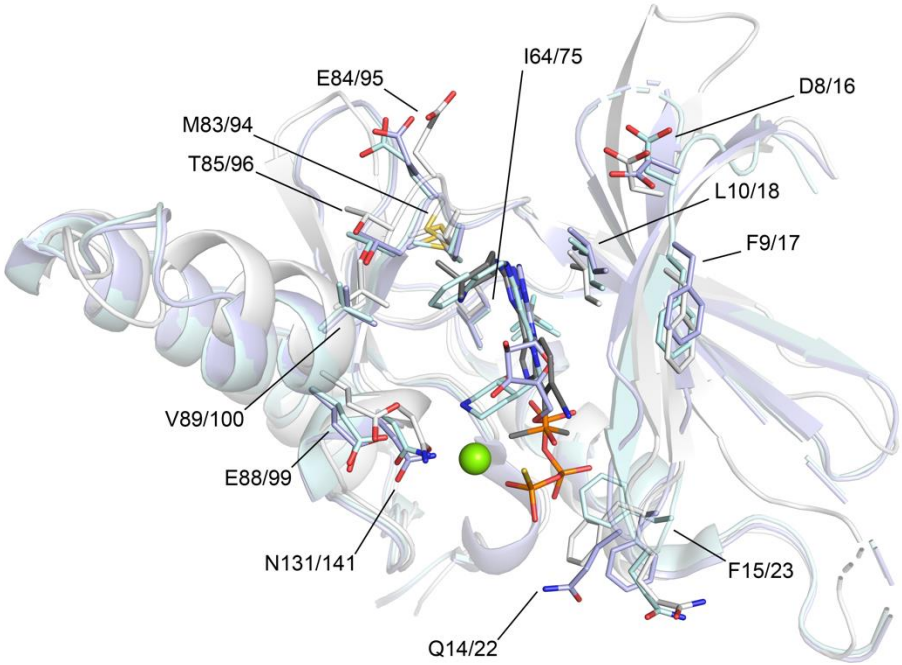

Figure 6. Structural comparison of CDK2m7 and CDK7. Structural alignment of N-terminal portions of CDK2m7 with SY5609 (grey) and CDK7 with Samuraciclib (PDB 8p6v, cyan) and CDK7 with an ATP analogue ATP-gamma-S (PDB 8p6y, violet). The green sphere represents a magnesium cation from PDB 8p6y. Mutated residues are shown as sticks with residue numbering indicated in the CDK2/CDK7 order.

CDK2m7 keeps the overall binding mode of the SY5609 inhibitor lineage

CDK7 inhibitors often exhibit affinity also to CDK2 and crystal structures of their complexes with CDK2 can be used as an approximation in structure-assisted development of CDK7 inhibitors. This was also the case in the design of inhibitor SY5609, where the predecessor compound 4 was crystallized with inactive, cyclin-free CDK2 (PDB 7ra5) [41]. Structural alignments revealed that SY5609 binds to CDK2m7 in an overall very similar pose as compound 4 to CDK2. A direct comparison of binding details is depicted in Figure 7; however,

we must keep in mind that the inactive monomeric CDK2 differs in conformation from the active, cyclin A-bound CDK2, which may affect how inhibitors bind to these two activation states [43]. Nevertheless, the comparison clearly indicates that CDK2m7 keeps the overall conserved binding mode of the SY5609 [41] lineage of inhibitors.

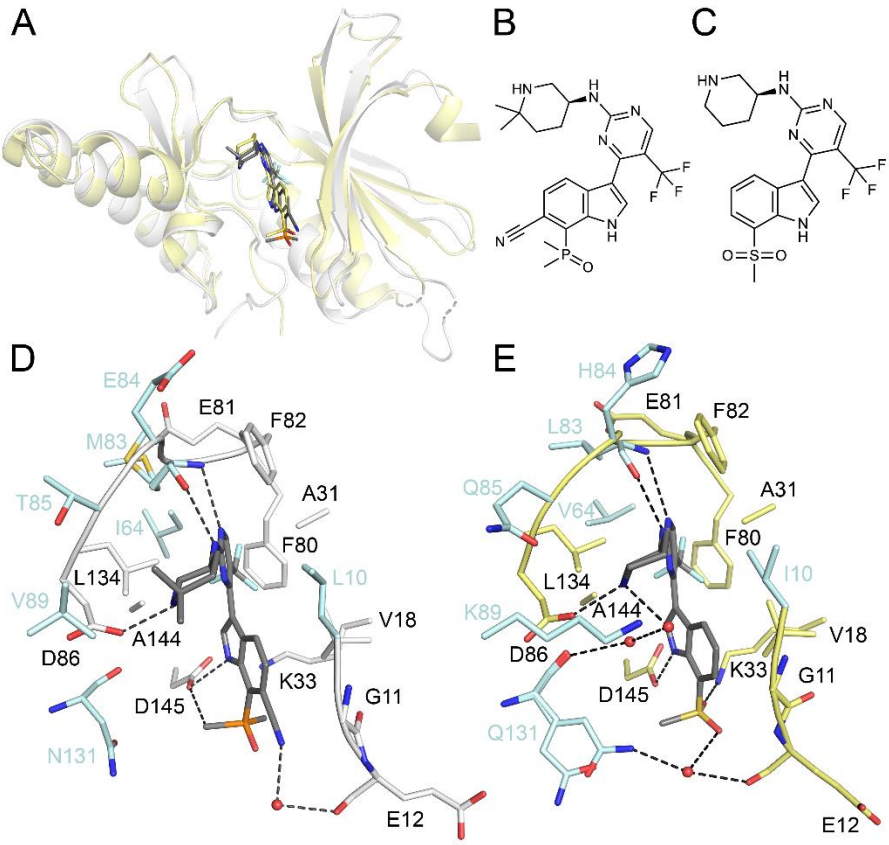

Figure 7. Structural comparison of the binding of SY5609 to CDK7 and compound 4 to CDK2. A. Structural alignment of N-terminal portions of CDK2m7 with SY5609 (grey) and CDK2 with compound 4 (PDB 7ra5, yellow) [41]. B. Chemical structure of SY5609. C. Chemical structure of compound 4. D. Interactions between CDK2m7 and SY5609. E. Interactions between CDK2 and compound 4. Hydrogen bonds are shown as dashed lines and water molecules as red spheres. Residues interacting with either of the inhibitors are shown as sticks and mutated residues are highlighted in cyan.

Crystal structure of CDK2m7/cycA/SY5609 supports the molecular docking model of CDK7/cycH/MAT1/SY5609

Binding of SY5609 to CDK7 was previously simulated by docking SY5609 into the structure of active CDK7 in complex with cyclin H and MAT1 (PDB 7b5q [20]) [41], followed by molecular dynamics simulations. The interactions with CDK7 predicted in the docking

experiments agree well with our structure. The interaction network is virtually unchanged in the hinge and gatekeeper region, including the main inhibitor scaffold. These interactions, however, are conserved between CDK2 and CDK7.

During the development of SY5609, modifications of positions 6 and 7 of the indole moiety and position 6 of the piperidine moiety appeared to play the greatest role in the shift of selectivity towards CDK7 over off-target CDKs [41]. The dimethyl modification of the 6-position of the piperidine moiety was suggested to improve the selectivity towards CDK7 by engaging the non-conserved Val100 in CDK7 [41] (K89V mutation in CDK2m7). Indeed, our structure confirms that the dimethyl group forms van der Waals interactions with Val89 in CDK2m7 and would potentially clash with Lys89 in CDK2.

Position 6 of the indole ring is modified with the nitrile moiety pointing towards the P-loop, and position 7 is modified by the dimethyl phosphine oxide, occupying the phosphate-binding sub-pocket and interacting with the catalytic Asp145. In the molecular modelling experiments, the nitrile moiety was suggested to interact transiently through water-mediated hydrogen bonds with the backbone carbonyl of Glu20 (Glu12 in CDK2m7). Our structure serves as an experimental proof of this interaction with the P-loop.

In the modeling approach, the conformation of SY5609 was constrained in a conformation observed in the small molecule X-ray structure of the inhibitor, preserving an internal hydrogen bond between the phosphine oxide and the indole NH group [41]. This conformation imparts favorable pharmacokinetic properties to SY5609, such as improved permeability. Docking of the inhibitor in this constrained conformation resulted in water-mediated hydrogen-bond interactions between the phosphine oxide and the catalytic Lys41 (Lys33 in CDK2m7) and Asp155 (Asp145 in CDK2m7). However, our structure shows that this conformation of the dimethyl phosphine oxide engaged in the internal hydrogen bond with the indole nitrogen is not favorable when bound in the active site of CDK2m7, because the oxygen atom would repulse with the side chain of the catalytic residue Asp145, which is held in place by a hydrogen bond and a salt bridge with catalytic Lys33. Asp145 rather forms a weak hydrogen bond with a methyl group of the dimethyl phosphine oxide. Such orientation of this methyl group is consistent with the structure of CDK2 with compound 4 [41] (Figure 7).

While the CDK2m7 protein presented in this work is an extensive active site mutant, in the light of new structural information, it can serve as a basis for the design of further mimic variants containing more amino acid substitutions. In particular, the glycine-rich loop is a candidate region to place substitutions in amino acid residues that are not in direct contact with

inhibitors but may influence the loop flexibility affecting thus ligand selectivity [20, 44]. For example, one such residue could be Ala24, that is unique to CDK7 and corresponds to Gly16 in CDK2, and was suggested to influence the flexibility of the glycine-rich loop [41].

During finalization of this publication, an alternative approach to high-throughput crystallographic analysis of CDK7 inhibitors was reported [45], presenting a back-soakable crystal form of monomeric CDK7 with two T-loop phospho-mimicking mutations and an engineered surface mutation resulting in crystal contacts that enable active kinase conformation. The authors also report a CDK2-7 chimera containing seven CDK7-specific ATP site mutations (I10L, T14Q, V64I, K88E, K89V, D92K, Q131N) that can be produced in *E. coli*. Contrary to our study, this chimera is a monomeric and inactive (non-phosphorylated) kinase with no cyclin bound and does not contain CDK7-mimic mutations in the inhibitor-binding hinge region. The CDK2m7 mimic presented here can be produced in *E. coli* and readily co-crystallized with CDK7 inhibitors, without the need of back-soaking that usually requires higher-affinity inhibitors. CDK2m7 thus represents a valuable tool for rapid and affordable assessment of both structural and functional aspects of CDK7 inhibitor binding.

In conclusion, CDK2m7 can be produced in *E. coli* in a fully active, phosphorylated form in complex with cyclin A2. The purification protocol provides a yield and purity suitable for X-ray crystallography. CDK2m7 exhibits a shift in selectivity from CDK2 to CDK7 and can therefore serve as a good mimic of CDK7 in structure-assisted design of CDK7 inhibitors. CDK2m7 represents a simple, widely available, and affordable model system for CDK7 drug development.

Data statement

The crystallographic data were deposited in the Protein Data Bank (https://www.rcsb.org/) under the accession code 9GLA.

Glossary

CDK active site pocket sub-sites, as defined for CDK2 [42]:

hinge-region: Glu81-Leu83;

gatekeeper residue: Phe80;

specificity-surface: residues Gln85, Asp86, and Lys89;

phosphate-ribose-binding pocket: outlined by residues Gly13, Lys129, and Gln131;

glycine-rich loop: Gly11-Gly16.

Abbreviations

CDK, cyclin-dependent kinase; cyc, cyclin; CDK2m7, CDK2-based CDK7 mimic

Declaration of competing interest

The authors declare that they have no known competing financial interests or personal relationships that could have appeared to influence the work reported in this paper.

Acknowledgements

We would like to thank Dr. Petr Pachl from IOCB Prague for diffraction data collection and Dr. Martin Lepšík of High Performance Computing Core Facility of IOCB Prague for advice on inhibitor geometry and binding. We acknowledge SOLEIL for provision of synchrotron radiation facilities and we would like to thank Dr. Martin Savko for assistance in using beamline PX2a. The work was supported by project National Institute for Cancer Research (Programme EXCELES, ID Project No. LX22NPO5102) - Funded by the European Union - Next Generation EU.

Author contributions

The manuscript was written through contributions of all authors. All authors have given approval to the final version of the manuscript.

CRediT authorship contribution statement

Jana Škerlová: Conceptualization, Formal analysis, Data curation, Writing – original draft, Writing – review & editing, Visualization, Supervision, Project administration. **Veronika Krejčiříková**: Investigation, Writing – original draft. **Miroslav Peřina**: Investigation. **Veronika Vojáčková**: Investigation. **Milan Fábry**: Investigation, Writing – original draft. **Vladimír Kryštof**: Writing – review & editing, Project administration, Funding acquisition. **Radek Jorda**: Investigation, Data curation, Writing – original draft, Visualization. **Pavlína Řezáčová**: Conceptualization, Writing – review & editing, Project administration, Funding acquisition.

References

[1] P.K. Parua, R.P. Fisher, Dissecting the Pol II transcription cycle and derailing cancer with CDK inhibitors, Nat Chem Biol 16(7) (2020) 716-724.
[2] S.J. Vervoort, J.R. Devlin, N. Kwiatkowski, M. Teng, N.S. Gray, R.W. Johnstone, Targeting transcription cycles in cancer, Nat Rev Cancer 22(1) (2022) 5-24.
[3] T. Lei, P. Zhang, X. Zhang, X. Xiao, J. Zhang, T. Qiu, Q. Dai, Y. Zhang, L. Min, Q. Li, R. Yin, P. Ding, N. Li, Y. Qu, D. Mu, J. Qin, X. Zhu, Z.X. Xiao, Q. Li, Cyclin K regulates prereplicative complex assembly to promote mammalian cell proliferation, Nat Commun 9(1) (2018) 1876.
[4] M.S. Akhtar, M. Heidemann, J.R. Tietjen, D.W. Zhang, R.D. Chapman, D. Eick, A.Z. Ansari, TFIIH kinase places bivalent marks on the carboxy-terminal domain of RNA polymerase II, Mol Cell 34(3) (2009) 387-93.
[5] K. Glover-Cutter, S. Larochelle, B. Erickson, C. Zhang, K. Shokat, R.P. Fisher, D.L. Bentley, TFIIH-associated Cdk7 kinase functions in phosphorylation of C-terminal domain

Ser7 residues, promoter-proximal pausing, and termination by RNA polymerase II, Mol Cell Biol 29(20) (2009) 5455-64.
[6] W. Shan, J. Yuan, Z. Hu, J. Jiang, Y. Wang, N. Loo, L. Fan, Z. Tang, T. Zhang, M. Xu, Y. Pan, J. Lu, M. Long, J.L. Tanyi, K.T. Montone, Y. Fan, X. Hu, Y. Zhang, L. Zhang, Systematic Characterization of Recurrent Genomic Alterations in Cyclin-Dependent Kinases Reveals Potential Therapeutic Strategies for Cancer Treatment, Cell Rep 32(2) (2020) 107884.
[7] M. Kovalova, J.P. Baraka, V. Mik, R. Jorda, L. Luo, H. Shao, V. Krystof, A patent review of cyclin-dependent kinase 7 (CDK7) inhibitors (2018-2022), Expert Opin Ther Pat 33(2) (2023) 67-87.
[8] S. Ali, D.A. Heathcote, S.H. Kroll, A.S. Jogalekar, B. Scheiper, H. Patel, J. Brackow, A. Siwicka, M.J. Fuchter, M. Periyasamy, R.S. Tolhurst, S.K. Kanneganti, J.P. Snyder, D.C. Liotta, E.O. Aboagye, A.G. Barrett, R.C. Coombes, The development of a selective cyclin-dependent kinase inhibitor that shows antitumor activity, Cancer Res 69(15) (2009) 6208-15.
[9] T.W. Kelso, K. Baumgart, J. Eickhoff, T. Albert, C. Antrecht, S. Lemcke, B. Klebl, M. Meisterernst, Cyclin-dependent kinase 7 controls mRNA synthesis by affecting stability of preinitiation complexes, leading to altered gene expression, cell cycle progression, and survival of tumor cells, Mol Cell Biol 34(19) (2014) 3675-88.
[10] H. Patel, M. Periyasamy, G.P. Sava, A. Bondke, B.W. Slafer, S.H.B. Kroll, M. Barbazanges, R. Starkey, S. Ottaviani, A. Harrod, E.O. Aboagye, L. Buluwela, M.J. Fuchter, A.G.M. Barrett, R.C. Coombes, S. Ali, ICEC0942, an Orally Bioavailable Selective Inhibitor of CDK7 for Cancer Treatment, Mol Cancer Ther 17(6) (2018) 1156-1166.
[11] N. Kwiatkowski, T. Zhang, P.B. Rahl, B.J. Abraham, J. Reddy, S.B. Ficarro, A. Dastur, A. Amzallag, S. Ramaswamy, B. Tesar, C.E. Jenkins, N.M. Hannett, D. McMillin, T. Sanda, T. Sim, N.D. Kim, T. Look, C.S. Mitsiades, A.P. Weng, J.R. Brown, C.H. Benes, J.A. Marto, R.A. Young, N.S. Gray, Targeting transcription regulation in cancer with a covalent CDK7 inhibitor, Nature 511(7511) (2014) 616-20.
[12] S. Hu, J.J. Marineau, N. Rajagopal, K.B. Hamman, Y.J. Choi, D.R. Schmidt, N. Ke, L. Johannessen, M.J. Bradley, D.A. Orlando, S.R. Alnemy, Y. Ren, S. Ciblat, D.K. Winter, A. Kabro, K.T. Sprott, J.G. Hodgson, C.C. Fritz, J.P. Carulli, E. di Tomaso, E.R. Olson, Discovery and Characterization of SY-1365, a Selective, Covalent Inhibitor of CDK7, Cancer Res 79(13) (2019) 3479-3491.
[13] C.M. Olson, Y. Liang, A. Leggett, W.D. Park, L. Li, C.E. Mills, S.Z. Elsarrag, S.B. Ficarro, T. Zhang, R. Duster, M. Geyer, T. Sim, J.A. Marto, P.K. Sorger, K.D. Westover, C.Y. Lin, N. Kwiatkowski, N.S. Gray, Development of a Selective CDK7 Covalent Inhibitor Reveals Predominant Cell-Cycle Phenotype, Cell Chem Biol 26(6) (2019) 792-803 e10.
[14] X. Song, C. Fang, Y. Dai, Y. Sun, C. Qiu, X. Lin, R. Xu, Cyclin-dependent kinase 7 (CDK7) inhibitors as a novel therapeutic strategy for different molecular types of breast cancer, Br J Cancer 130(8) (2024) 1239-1248.
[15] N.R. Brown, M.E. Noble, J.A. Endicott, L.N. Johnson, The structural basis for specificity of substrate and recruitment peptides for cyclin-dependent kinases, Nat Cell Biol 1(7) (1999) 438-43.
[16] H.M. Berman, J. Westbrook, Z. Feng, G. Gilliland, T.N. Bhat, H. Weissig, I.N. Shindyalov, P.E. Bourne, The Protein Data Bank, Nucleic Acids Res 28(1) (2000) 235-42.
[17] G. Lolli, E.D. Lowe, N.R. Brown, L.N. Johnson, The crystal structure of human CDK7 and its protein recognition properties, Structure 12(11) (2004) 2067-79.
[18] B.J. Greber, J.M. Perez-Bertoldi, K. Lim, A.T. Iavarone, D.B. Toso, E. Nogales, The cryoelectron microscopy structure of the human CDK-activating kinase, Proc Natl Acad Sci U S A 117(37) (2020) 22849-22857.

[19] R. Duster, K. Anand, S.C. Binder, M. Schmitz, K. Gatterdam, R.P. Fisher, M. Geyer, Structural basis of Cdk7 activation by dual T-loop phosphorylation, Nat Commun 15(1) (2024) 6597.
[20] B.J. Greber, J. Remis, S. Ali, E. Nogales, 2.5 A-resolution structure of human CDK-activating kinase bound to the clinical inhibitor ICEC0942, Biophys J 120(4) (2021) 677-686.
[21] V.I. Cushing, A.F. Koh, J. Feng, K. Jurgaityte, A. Bondke, S.H.B. Kroll, M. Barbazanges, B. Scheiper, A.K. Bahl, A.G.M. Barrett, S. Ali, A. Kotecha, B.J. Greber, High-resolution cryo-EM of the human CDK-activating kinase for structure-based drug design, Nat Commun 15(1) (2024) 2265.
[22] M. Ikuta, K. Kamata, K. Fukasawa, T. Honma, T. Machida, H. Hirai, I. Suzuki-Takahashi, T. Hayama, S. Nishimura, Crystallographic approach to identification of cyclin-dependent kinase 4 (CDK4)-specific inhibitors by using CDK4 mimic CDK2 protein, J Biol Chem 276(29) (2001) 27548-54.
[23] M. Gassel, C.B. Breitenlechner, P. Ruger, U. Jucknischke, T. Schneider, R. Huber, D. Bossemeyer, R.A. Engh, Mutants of protein kinase A that mimic the ATP-binding site of protein kinase B (AKT), J Mol Biol 329(5) (2003) 1021-34.
[24] S. Bonn, S. Herrero, C.B. Breitenlechner, A. Erlbruch, W. Lehmann, R.A. Engh, M. Gassel, D. Bossemeyer, Structural analysis of protein kinase A mutants with Rho-kinase inhibitor specificity, J Biol Chem 281(34) (2006) 24818-30.
[25] Y. Lu, M. Knapp, K. Crawford, R. Warne, R. Elling, K. Yan, M. Doyle, G. Pardee, L. Zhang, S. Ma, M. Mamo, E. Ornelas, Y. Pan, D. Bussiere, J. Jansen, I. Zaror, A. Lai, P. Barsanti, J. Sim, Rationally Designed PI3Kalpha Mutants to Mimic ATR and Their Use to Understand Binding Specificity of ATR Inhibitors, J Mol Biol 429(11) (2017) 1684-1704.
[26] A. Echalier, E. Cot, A. Camasses, E. Hodimont, F. Hoh, P. Jay, F. Sheinerman, L. Krasinska, D. Fisher, An integrated chemical biology approach provides insight into Cdk2 functional redundancy and inhibitor sensitivity, Chem Biol 19(8) (2012) 1028-40.
[27] W. Kabsch, Xds, Acta Crystallogr D Biol Crystallogr 66(Pt 2) (2010) 125-32.
[28] A. Vagin, A. Teplyakov, Molecular replacement with MOLREP, Acta Crystallogr D Biol Crystallogr 66(Pt 1) (2010) 22-5.
[29] R. Jorda, L. Havlicek, M. Perina, V. Vojackova, T. Pospisil, S. Djukic, J. Skerlova, J. Gruz, N. Renesova, P. Klener, P. Rezacova, M. Strnad, V. Krystof, 3,5,7-Substituted Pyrazolo[4,3-d]Pyrimidine Inhibitors of Cyclin-Dependent Kinases and Cyclin K Degraders, J Med Chem 65(13) (2022) 8881-8896.
[30] G.N. Murshudov, A.A. Vagin, E.J. Dodson, Refinement of macromolecular structures by the maximum-likelihood method, Acta Crystallogr D Biol Crystallogr 53(Pt 3) (1997) 240-55.
[31] M.D. Winn, C.C. Ballard, K.D. Cowtan, E.J. Dodson, P. Emsley, P.R. Evans, R.M. Keegan, E.B. Krissinel, A.G. Leslie, A. McCoy, S.J. McNicholas, G.N. Murshudov, N.S. Pannu, E.A. Potterton, H.R. Powell, R.J. Read, A. Vagin, K.S. Wilson, Overview of the CCP4 suite and current developments, Acta Crystallogr D Biol Crystallogr 67(Pt 4) (2011) 235-42.
[32] P. Emsley, K. Cowtan, Coot: model-building tools for molecular graphics, Acta Crystallogr D Biol Crystallogr 60(Pt 12 Pt 1) (2004) 2126-32.
[33] N.W. Moriarty, R.W. Grosse-Kunstleve, P.D. Adams, electronic Ligand Builder and Optimization Workbench (eLBOW): a tool for ligand coordinate and restraint generation, Acta Crystallogr D Biol Crystallogr 65(Pt 10) (2009) 1074-80.
[34] D. Liebschner, P.V. Afonine, M.L. Baker, G. Bunkoczi, V.B. Chen, T.I. Croll, B. Hintze, L.W. Hung, S. Jain, A.J. McCoy, N.W. Moriarty, R.D. Oeffner, B.K. Poon, M.G. Prisant, R.J. Read, J.S. Richardson, D.C. Richardson, M.D. Sammito, O.V. Sobolev, D.H. Stockwell, T.C. Terwilliger, A.G. Urzhumtsev, L.L. Videau, C.J. Williams, P.D. Adams, Macromolecular structure determination using X-rays, neutrons and electrons: recent developments in Phenix, Acta Crystallogr D Struct Biol 75(Pt 10) (2019) 861-877.

[35] R. Jorda, D. Hendrychova, J. Voller, E. Reznickova, T. Gucky, V. Krystof, How Selective Are Pharmacological Inhibitors of Cell-Cycle-Regulating Cyclin-Dependent Kinases?, J Med Chem 61(20) (2018) 9105-9120.
[36] E.B. Faber, L. Sun, J. Tang, E. Roberts, S. Ganeshkumar, N. Wang, D. Rasmussen, A. Majumdar, L.E. Hirsch, K. John, A. Yang, H. Khalid, J.E. Hawkinson, N.M. Levinson, V. Chennathukuzhi, D.A. Harki, E. Schonbrunn, G.I. Georg, Development of allosteric and selective CDK2 inhibitors for contraception with negative cooperativity to cyclin binding, Nat Commun 14(1) (2023) 3213.
[37] F. Madeira, M. Pearce, A.R.N. Tivey, P. Basutkar, J. Lee, O. Edbali, N. Madhusoodanan, A. Kolesnikov, R. Lopez, Search and sequence analysis tools services from EMBL-EBI in 2022, Nucleic Acids Res 50(W1) (2022) W276-W279.
[38] L.T. Vassilev, C. Tovar, S. Chen, D. Knezevic, X. Zhao, H. Sun, D.C. Heimbrook, L. Chen, Selective small-molecule inhibitor reveals critical mitotic functions of human CDK1, Proc Natl Acad Sci U S A 103(28) (2006) 10660-5.
[39] B. Wang, J. Wu, Y. Wu, C. Chen, F. Zou, A. Wang, H. Wu, Z. Hu, Z. Jiang, Q. Liu, W. Wang, Y. Zhang, F. Liu, M. Zhao, J. Hu, T. Huang, J. Ge, L. Wang, T. Ren, Y. Wang, J. Liu, Q. Liu, Discovery of 4-(((4-(5-chloro-2-(((1s,4s)-4-((2-methoxyethyl)amino)cyclohexyl)amino)pyridin-4-yl)thiazol-2-yl)amino)methyl)tetrahydro-2H-pyran-4-carbonitrile (JSH-150) as a novel highly selective and potent CDK9 kinase inhibitor, Eur J Med Chem 158 (2018) 896-916.
[40] C.R. Coxon, E. Anscombe, S.J. Harnor, M.P. Martin, B. Carbain, B.T. Golding, I.R. Hardcastle, L.K. Harlow, S. Korolchuk, C.J. Matheson, D.R. Newell, M.E. Noble, M. Sivaprakasam, S.J. Tudhope, D.M. Turner, L.Z. Wang, S.R. Wedge, C. Wong, R.J. Griffin, J.A. Endicott, C. Cano, Cyclin-Dependent Kinase (CDK) Inhibitors: Structure-Activity Relationships and Insights into the CDK-2 Selectivity of 6-Substituted 2-Arylaminopurines, J Med Chem 60(5) (2017) 1746-1767.
[41] J.J. Marineau, K.B. Hamman, S. Hu, S. Alnemy, J. Mihalich, A. Kabro, K.M. Whitmore, D.K. Winter, S. Roy, S. Ciblat, N. Ke, A. Savinainen, A. Wilsily, G. Malojcic, R. Zahler, D. Schmidt, M.J. Bradley, N.J. Waters, C. Chuaqui, Discovery of SY-5609: A Selective, Noncovalent Inhibitor of CDK7, J Med Chem 65(2) (2022) 1458-1480.
[42] M. Hylsova, B. Carbain, J. Fanfrlik, L. Musilova, S. Haldar, C. Kopruluoglu, H. Ajani, P.S. Brahmkshatriya, R. Jorda, V. Krystof, P. Hobza, A. Echalier, K. Paruch, M. Lepsik, Explicit treatment of active-site waters enhances quantum mechanical/implicit solvent scoring: Inhibition of CDK2 by new pyrazolo[1,5-a]pyrimidines, Eur J Med Chem 126 (2017) 1118-1128.
[43] G. Kontopidis, C. McInnes, S.R. Pandalaneni, I. McNae, D. Gibson, M. Mezna, M. Thomas, G. Wood, S. Wang, M.D. Walkinshaw, P.M. Fischer, Differential binding of inhibitors to active and inactive CDK2 provides insights for drug design, Chem Biol 13(2) (2006) 201-11.
[44] P. Hazel, S.H. Kroll, A. Bondke, M. Barbazanges, H. Patel, M.J. Fuchter, R.C. Coombes, S. Ali, A.G. Barrett, P.S. Freemont, Inhibitor Selectivity for Cyclin-Dependent Kinase 7: A Structural, Thermodynamic, and Modelling Study, ChemMedChem 12(5) (2017) 372-380.
[45] M. Mukherjee, P.J. Day, D. Laverty, J.A. Bueren-Calabuig, A.J. Woodhead, C. Griffiths-Jones, S. Hiscock, C. East, S. Boyd, M. O'Reilly, Protein engineering enables a soakable crystal form of human CDK7 primed for high-throughput crystallography and structure-based drug design, Structure 32(8) (2024) 1040-1048 e3.